Numerical Investigation of Fibers Effects in SFRC under Dynamic Tension

Numerical Investigation of Fibers Effects in SFRC under Dynamic Tension

Y. CAO[a], Q.L. YU[a], H.J.H. BROUWERS[a]
[a] Department of the Built Environment, Eindhoven University of Technology,
P.O. Box 513, 5600 MB Eindhoven, the Netherlands

Abstract: This study investigates the effects of fibers in steel fiber reinforced concrete (SFRC) on its mechanical properties and failure processes under different loading rates using LS-DYNA. A single fiber pullout test is simulated first to validate the material models and parameters used in the numerical simulations. After the validation, SFRC specimen with a single steel fiber under uniaxial tension is modelled at the mesoscale to present the failure process and the crack development in the specimen. The effects of fibers and the strain rate on the strength, stiffness and toughness of the SFRC are analyzed based on the stress-strain curves. Then SFRC specimens with multiple steel fibers are modelled. The effects of the fiber content on the dynamic properties of the SFRC specimen, such as the dynamic increase factor of its tensile resistance, are evaluated. The simulation results show that the mechanical properties of SFRC can be influenced by both the steel fiber content and the loading rate. The incorporation of steel fibers can lead to an increase of the maximum tensile resistance, the corresponding yield displacement as well as the fracture energy of the SFRC specimens; however the rate-sensitivity is less significant at higher fiber volume content.

Keywords: SFRC; dynamic tension; numerical simulation; failure process

1 Introduction

As a brittle material, traditional concrete is characterized by its low tensile strength, low fracture toughness and poor resistance to crack growth [1-4]. The addition of steel fibers in the cement matrix has been recognized to be an effective methodology for enhancing the post-cracking response of concrete. Fiber reinforcements, acting as stress-transfer bridges, can restrain the propagation of cracks at both micro- and macro-levels, thus endowing substantially higher energy absorption capacity and toughness. For micro-cracks, fibers abate their initiation and growth by providing crack tip plasticity and increased fracture toughness; while for macro-cracks, fibers can provide effective bridging, inhibit their unstable propagation, and act as sources of strength gain, toughness and ductility [2-4]. As a consequence, the behavior of steel fiber reinforced concrete (SFRC) is superior to that of plain concrete. The significantly enhanced tensile strength, post-cracking ductility, energy absorption capacity, as well as the crack control ability of SFRC [2, 3, 5-8] contribute to its wide use throughout the world, especially for structures resist dynamic loadings.

The behavior of cement-based material subjected to dynamic loading is different from that under static loading due to the strain rate effect. The response of SFRC under static loadings has been extensively investigated over the past several decades [5-10], while its dynamic response is relatively less reported in literatures. Among the limited researches, Mohammadi et al. [11] studied the impact resistance of SFRC containing fibers of mixed aspect ratio with drop weight experiments. They evaluated the impact energy at first crack and ultimate failure, and obtained that SFRC with 2.0% long fibers showed the best performance under the impact loading. Wang et al. [12] experimentally investigated the dynamic behaviors of SFRC with split Hopkinson pressure bar, and found that the toughness energy is proportional to the fiber content. Considering the increasing risks of structural failures under dynamic loadings in occasions such as terrorist attacks and accidental impacts, an in-depth understanding of the response of SFRC subjected to dynamic loading is necessary.

With the advancement of computer technology, numerical simulation of SFRC under dynamic loading has become feasible. Most numerical simulations are at macroscale, in which SFRC is modelled as a homogeneous material and the effect of fibers are accounted by modifying the softening law in plain concrete models. For example, Wang et al. [13] simulated the perforation in SFRC targets under penetrations using LS-DYNA. The softening behavior of the SFRC target is modelled with different effective stress-effective plastic strain relations which vary with different fiber aspect ratios. Similar macroscale simulations were done by Teng et al. [14]. On the other hand, mesoscale modelling, providing more realistic representation of concrete heterogeneity, can yield more realistic simulations of material failure mechanisms [15]. Thus numerical simulations at mesoscale can help to give insight into the effects of fibers in SFRC on the mechanical properties and failure processes of the composite.

The objective of this study is to investigate the effects of fibers in SFRC under dynamic tensile loads with various strain rates. Fibers in the SFRC specimens are explicitly present with mesoscale models, thus the dynamic mechanical properties and the failure processes of the specimens are analyzed in a more direct means. The material models and related parameters are validated by a single fiber pullout simulation first. Then notched SFRC specimens reinforced with single and multiple steel fibers are modeled in the simulation program. Fibers effects are evaluated in terms of the failure processes, the specimen performance, e.g. the maximum tensile strength, yield displacement and energy absorption capacity, as well as

the rate sensitivity. This study advances the fundamental understanding of the effects of fibers on the tensile behavior of SFRC under dynamic loadings.

2 Material models and pullout validation

2.1 Material models

In this study, numerical models of SFRC specimens are constructed in LS-DYNA. To better understand the effects of fibers, the current work explicitly models the fiber inclusions in the SFRC. Moreover, the interface zone (ITZ) between the fiber and the matrix is also explicitly presented in the simulations since the properties of ITZ are reported to significantly affect the bond between the fiber and its surrounding matrix [16]. Considering the calculation efficiency, aggregates and cement matrix are taken into account together as one homogeneous material, i.e. concrete, and the total effects of the aggregates and the cement are considered by adjusting parameters in the concrete material model. Therefore, the SFRC model in this study is composed of three parts: the fibers, the concrete (including the aggregates and cement matrix), and the interface zone between the fiber and the concrete (ITZ).

For the steel fiber, a basic plastic kinematic model (MAT_3) is adopted due to its simplicity and adequate accuracy. The rate effect of steel fiber is not accounted in this study due to the lack of related data.

For the concrete and the ITZ, a plasticity with damage model (MAT_81) is employed. This material model provides access for users to define the non-linear visco-plastic softening behavior of the material with piecewise linear curves, and accounts for the effects of damage based on an effective plastic strain measure (Figure 1). The amount of damage evolved is represented by a constant ω which is defined as follows [17]:

$$\omega = \frac{\varepsilon^{\mathrm{p}}_{\mathrm{eff}} - \varepsilon^{\mathrm{p}}_{\mathrm{failure}}}{\varepsilon^{\mathrm{p}}_{\mathrm{rupture}} - \varepsilon^{\mathrm{p}}_{\mathrm{failure}}}, \quad \varepsilon^{\mathrm{p}}_{\mathrm{failure}} < \varepsilon^{\mathrm{p}}_{\mathrm{eff}} < \varepsilon^{\mathrm{p}}_{\mathrm{rupture}}$$

where $\varepsilon^{\mathrm{p}}_{\mathrm{eff}}$ is the effective plastic strain, $\varepsilon^{\mathrm{p}}_{\mathrm{failure}}$ is the effective plastic strain at which failure begins (ω=0), and $\varepsilon^{\mathrm{p}}_{\mathrm{rupture}}$ is the effective plastic strain at which the material ruptures (ω=1).

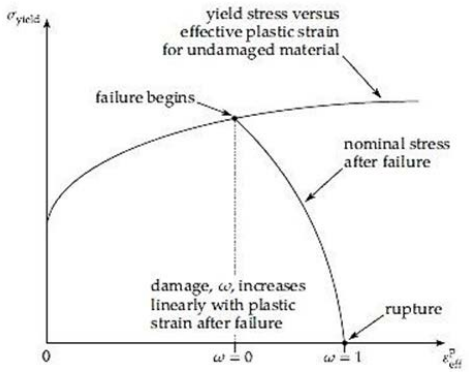

Fig. 1 Stress-strain behavior of MAT_81 [17]

The rate effects of the concrete and the ITZ are accounted into the plasticity with damage model using a dynamic increase factor (DIF) to scale the yield stress. In this study, the determinations of DIF are based on the recommendations in the CEB-FIB Model Code [18], which is the most widely adopted model accounting for the strain rate effects on mechanical properties of concrete:

Compression:

$$\mathrm{DIF} = \left(\frac{\dot{\varepsilon}_c}{\dot{\varepsilon}_{c0}}\right)^{1.026\alpha} \qquad \text{for } \dot{\varepsilon}_c \le 30\mathrm{s}^{-1}$$

$$\mathrm{DIF} = \gamma_c \left(\frac{\dot{\varepsilon}_c}{\dot{\varepsilon}_{c0}}\right)^{1/3} \qquad \text{for } \dot{\varepsilon}_c > 30\mathrm{s}^{-1}$$

where $\dot{\varepsilon}_c$ is the compressive strain rates, the static reference rate $\dot{\varepsilon}_{c0}$= 30 ×10^{-6} s^{-1}, α = 1/ (5+9f_{cu}/10), log γ_{c}=6.156α-2, f_{cu} is the static compressive strength (in MPa).

Tension:

$$\mathrm{DIF} = \left(\frac{\dot{\varepsilon}_t}{\dot{\varepsilon}_{t0}}\right)^{1.016\delta} \qquad \text{for } \dot{\varepsilon}_t \le 30\mathrm{s}^{-1}$$

$$\text{DIF} = \beta_t \left(\frac{\dot{\varepsilon}_t}{\dot{\varepsilon}_{t0}}\right)^{1/3} \quad \text{for } \dot{\varepsilon}_t > 30\text{s}^{-1}$$

where $\dot{\varepsilon}_t$ is the tensile strain rates, $\dot{\varepsilon}_{t0}$= 3 ×10^{-6} s^{-1}, δ = 1/ (10+3f_{cu}/5), log β_c=7.112δ-2.33.

Elements erosion of the concrete and the ITZ are also incorporated in the simulations with *MAT_ADD_EROSION, which provides a more direct way of including and controlling element failures in the plasticity with damage model. A maximum effective strain (ε_{eff}) failure criterion is applied to govern the erosion of the concrete material, i.e. erosion would happen when the effective strain in an element exceeds the setting failure strain. After the element erosion, it will be taken out and not be able to sustain any strength. The erosion of the ITZ is based on the minimum pressure failure (P_{min}) criteria to simulate the debonding of fibers and the surrounding concrete.

2.2 Simulation of single fiber pullout test

As the basic case, a straight single fiber pullout test conducted by Cunha et al. [19] is first simulated for the calibration and validation of parameters in the material models. The specimen for the pullout test is shown in Figure 2. Both the diameter and height of the concrete cylindrical are 80 mm, and the average compressive strength of the concrete is 83.4 MPa. The straight steel fiber adopted in the test has a length of 60 mm, a diameter of 0.75 mm and a yield stress of 1100 MPa [19].

2D Axisymmetric solid elements are used in the pullout simulation, and half of the specimen is modeled to save the computing time, as shown in Figure 3. In addition, the thickness of the ITZ is reported to have a value in the order of 40-70μm [20]; however, due to the difficulties in computing capacity, the ITZ is modeled to be 125 μm thick, which is also the smallest element length in this simulation. The material models and related parameters for the steel fiber, the concrete and the ITZ are given in Table 1.

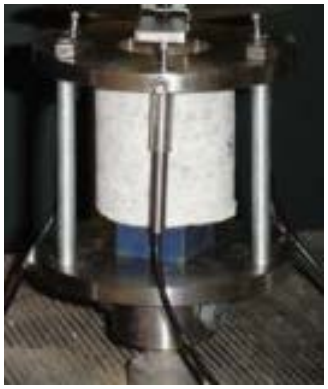

Fig. 2 The single fiber pullout test [19]

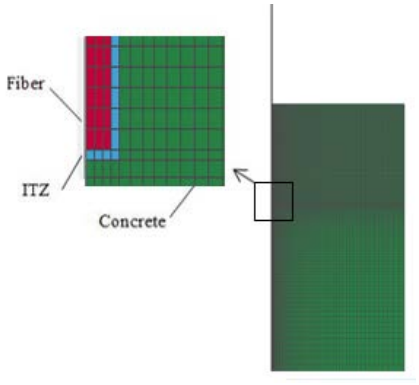

Fig. 3 2D Axisymmetric model

Table 1 Parameters for material models

	Material Models	Density (kg/m^3)	Young's modulus (GPa)	Yield strength (MPa)	Erosion criteria
Steel fiber	MAT_3	7800	210	1100	-
Concrete	MAT_81	2200	30	5	ε_{eff} =0.015
ITZ	MAT_81	2200	15	3	P_{min}=-2e7

To validate these material models and parameters, the single straight fiber pullout with an embedded fiber length of 30 mm is simulated [19]. The pullout force-end slip relations from the test and the simulation are compared and illustrated in Figure 4, in which only small differences exist between the descending parts of the two curves. It can be observed that with the calibrated parameters, the simulation result agrees well with the experimental values, which indicates the appropriation of the applied material models and parameters. Thus, these material models and parameters are further incorporated in the following analysis of the fibers effects on the dynamic mechanical properties and failure processes of the SFRC specimens under different loading rates.

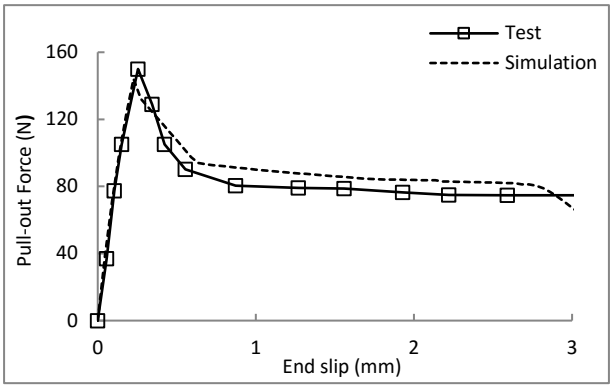

Fig. 4 Comparison of simulation results and test results

3 Effects of fibers under dynamic loading

3D models of notched SFRC specimens with fibers explicitly presented are built in LS-DYNA to analyze the effects of fibers and loading rates. The dimensions of the specimen are 50 × 30 × 2 mm^3. The length and width of the notch are 3 mm and 0.5 mm, respectively. To present the crack developments clearly as well as to save computing time, half of the specimen is modeled, i.e. the thickness of the model is 1 mm. Specimens with different amounts of fibers are considered in the simulations to investigate the influence of fiber volume fraction V_f. As shown in Figure 5, the green region represents the concrete, the red region is the fiber and the blue region represents the ITZ. The thickness of the ITZ and the diameter of the fiber are the same as those in the above pullout simulation. The length of the fiber equals to the embedded fiber length in the pullout simulation, i.e. l = 30 mm. The element used in the models is 3D tetrahedron, and the mesh is refined in the area near the notches considering that cracks tend to onset in these regions. The specimens are loaded at the upper and lower boundaries with a constant velocity $v = \dot{\varepsilon}h/2$, in which $\dot{\varepsilon}$ is the strain rate (1/s), h is the height of the specimen h = 50 mm.

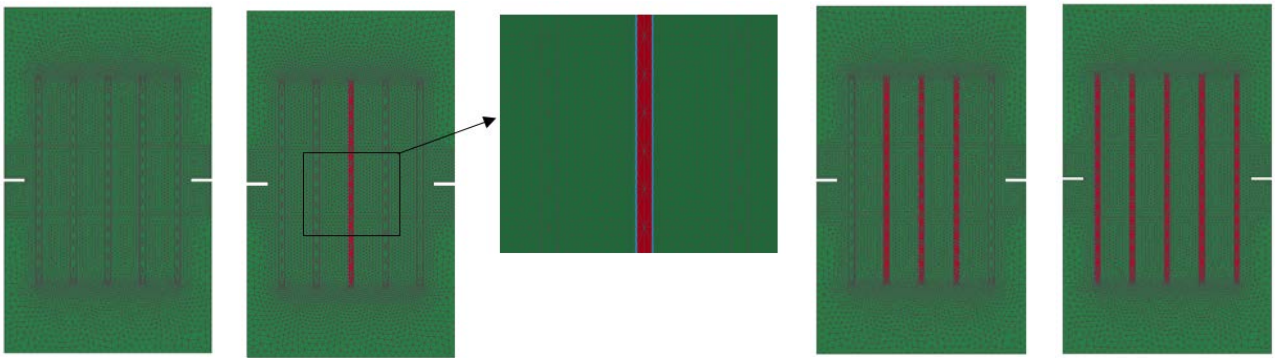

(a) V_f =0 (b) V_f =0.4% (c) V_f = 1.3% (d) V_f =2.2%

Fig. 5 3D models of specimens with different fiber volume fractions

3.1 Effects of single fiber under dynamic tension

The effect of single fiber is first analyzed by comparing the force-displacement relations of the plain concrete (V_f =0) and the single fiber concrete specimen (V_f =0.4%), as plotted in Figure 6. Both the lower loading rate case v=0.001m/s ($\dot{\varepsilon}$=0.04 /s) and the higher loading rate case v=0.1m/s ($\dot{\varepsilon}$=4 /s) are given in this figure. It is obvious that the maximum tensile strength is enhanced as the loading rate increases for both the plain concrete and the single fiber reinforced concrete specimen. Moreover, the comparison between these two specimens under v=0.001m/s indicates that the incorporation of the single fiber leads to increases of the maximum tensile resistance, the corresponding yield displacement as well as the fracture energy, which can be represented by the area below the force-displacement curve. Under the higher loading rate v=0.1m/s, the fracture energy and the strain capacity of the single fiber concrete specimen are also higher than those of the plain concrete specimen, which indicates a better energy absorption capacity and durability of the SFRC. However, the effects of the single fiber on the maximum tensile strength and the corresponding yield displacement are not very obvious under v=0.1m/s, i.e. the results are close for the SFRC and the plain concrete specimen. One possible reason for these slight differences may be that the material model of the steel fiber applied in

the simulations is rate-insensitive, which may result in underestimating the rate effects of the single fiber concrete specimen. These results also suggest that under higher loading rates, the rate effect of the concrete material is the dominant factor that influences the maximum tensile resistance of the specimen, and it plays a more significant role than the single steel fiber.

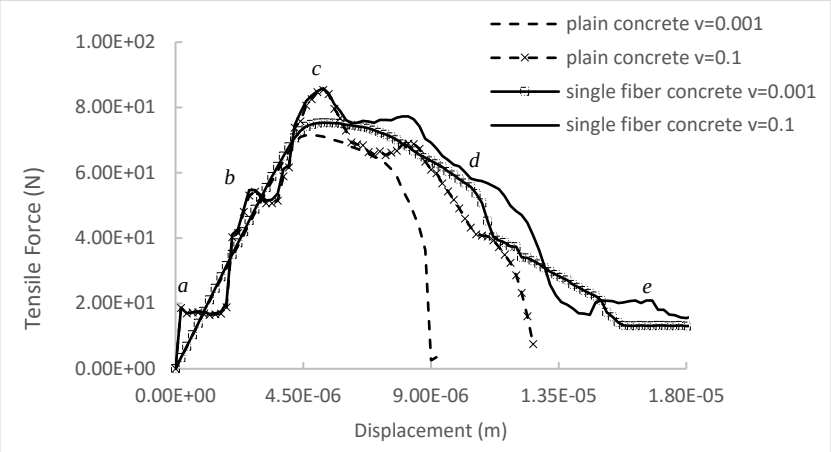

Fig. 6 Comparison of force-displacement relation

The failure processes in the single fiber concrete specimen under the loading v=0.1m/s are depicted in Figure 7 as an example. The letters *a*-*e* below the images identify different loading stages where the corresponding effective plastic strain distribution is taken. These stages also correspond to the points marked at the solid curve in Figure 6. As presented in Figure 7, the whole specimen was in a linear elastic regime before around t=10μs (Stage a), after which plastic strain localized near the notches and the tensile stress increased in a nonlinear way (Stage b). At around t=55μs (Stage c), the tensile stress reached its peak. In this stage, the plastic strain developed near the notches was more pronounced, accompanying with the erosion of some concrete elements in these areas. The existence of the fiber affected the wave propagation and reflection in the specimen and caused strain localizations in the concrete near the fiber ends. As the tensile load continued, more elements were damaged and cracks extended perpendicularly to the load direction, leading to the reduction of the specimen load carrying capacity (Stage d). At around t=175μs (Stage e), the strain localization process was almost completed, the main crack was almost fully developed, splitting the specimen into two pieces. After this stage, the two pieces of the SFRC specimen were connected together only by the steel fiber. Because of the fiber's connecting function, it was still possible for the specimen to bear some further load, thus the force-displacement curve in Figure 6 still showed a residual, not null, structural load carrying capacity after Stage e.

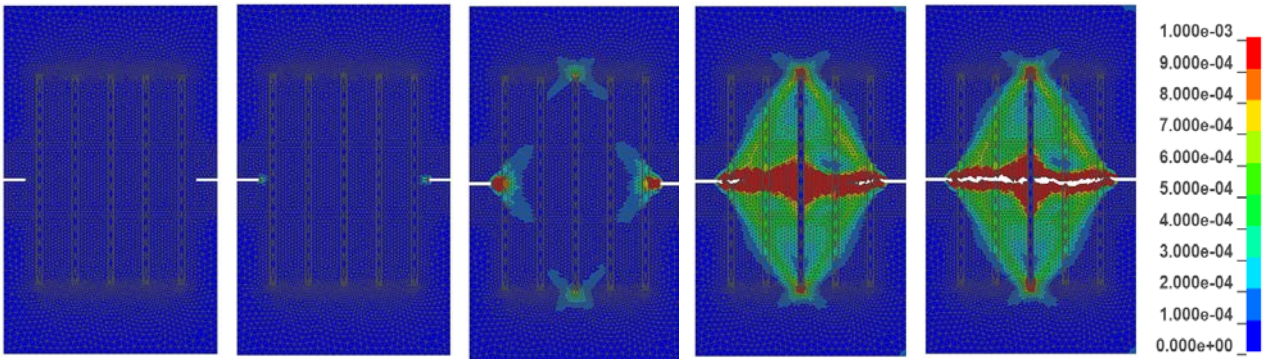

(a) t=10μs (b) t=30μs (c) t=55μs (d) t=115μs (e) t=175μs

Fig. 7 Different stages of effective plastic strain distribution

3.2 Effects of multiple fibers under dynamic tension

The effects of multiple fibers on the force-displacement relations at loading rate v=0.001m/s ($\dot{\varepsilon}$=0.04 /s) and v=0.1m/s ($\dot{\varepsilon}$=4 /s) are given in Figure 8. Clearly, under both loading rates, the maximum tensile strength of the SFRC specimen increases with the increase of fiber volume fraction V_f, while the elastic modulus is almost not influenced. The energy absorption capacity and the strain capacity of the SFRC specimen are also enhanced with the incorporation of the steel fibers.

Figure 9 illustrates the effects of fiber volume fraction and strain rate on the maximum tensile strength. It can be observed that the tensile resistance of the specimens increase with the increases in both fiber volume fraction and strain rate under the given loading rates. Moreover, the effect of fiber volume fraction on the maximum tensile strength seems to be more obvious for SFRC specimen under lower loading rates. For example, under loading rate v=0.001m/s, increasing the fiber volume fraction from 0 to 2.2% results in an approximate 14% increase of the maximum tensile strength, while for loading rate v=0.5m/s the corresponding increase is only about 3%.

Plots of dynamic increase factor versus strain rate for the tensile resistance of the SFRC specimens with different fiber volume fractions are presented in Figure 10. The dynamic increase factor is evaluated by comparing the maximum tension force under loading strain rates $\dot{\varepsilon}$=0.4 /s, 4/s, 12/s and 20/s (v=0.01m/s, 0.1m/s, 0.3m/s and 0.5m/s) with that of $\dot{\varepsilon}$=0.04 /s (v=0.001m/s), which is taken as the reference tensile force. As illustrated in the figure, the dynamic increase factor is higher for SFRC specimens with a lower fiber content, which indicates that the SFRC is less rate-sensitive than the plain concrete in the present simulations. Same tendency was reported by experimental studies in literatures [21, 22]. As mentioned earlier, this may be caused by the rate-independent material model applied for the steel fiber in our numerical simulations. In addition, under higher strain rates, e.g. $\dot{\varepsilon}$=20 /s, the maximum tensile strengths for the four plotted specimens are close to each other, which can also be observed in Figure 9 (the v=0.5m/s curve); while the reference tensile force is higher for the SFRC specimen reinforced with more steel fibers (see the v=0.001m/s curve in Figure 9), this may also contribute to the lower dynamic increase factor of the higher fiber concrete specimen.

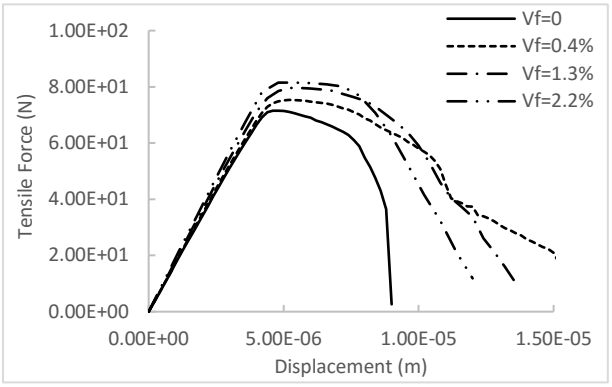

（a）loading rate v=0.001m/s

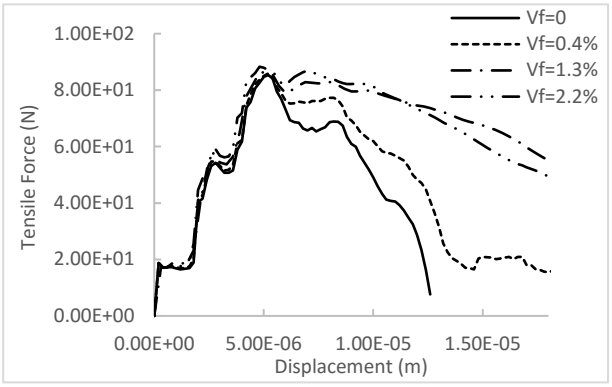

(b) loading rate v=0.1m/s

Fig. 8 Effect of fiber volume fractions on force-displacement relation

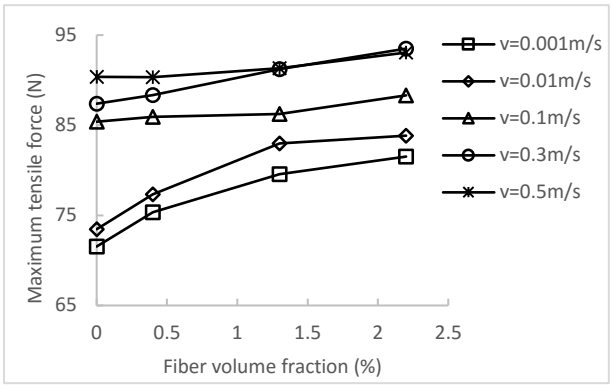

Fig. 9 Effect of fiber volume fraction on maximum tensile strength

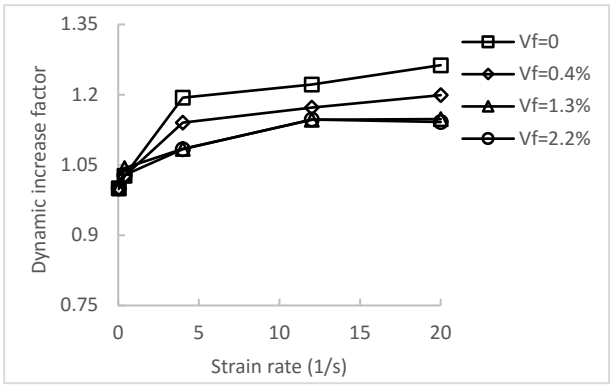

Fig. 10 Effect of fiber volume fraction on dynamic increase factor

4 Conclusions

In this study, mesoscale numerical simulations of SFRC specimens under dynamic tension at various loading rates are conducted. The steel fibers are explicitly presented in the models and their effects on the dynamic properties and failure processes of the SFRC specimens are analyzed. From the simulation results, the following observations and findings can be summarized:

(1) The increase in the loading rates leads to increases in the maximum tensile strength, corresponding to yield

displacement and the fracture energy of the SFRC specimen.

(2) The incorporation of steel fibers enhances the load carrying capacity, strain capacity and energy absorption capacity of the SFRC specimen under low loading rates.

(3) Under higher loading rates, the energy absorption capacity and strain capacity of the SFRC specimen increase with the fiber volume fraction; however, the influence of steel fiber on the tensile resistance is less pronounced, while the rate effect is the dominant factor for the increase of the tensile strength of the SFRC specimen.

(4) SFRC specimen with a higher fiber volume fraction is less rate-sensitive than that with lower fiber volume fraction.

(5) Steel fibers can influence the wave propagation and reflection in SFRC specimens and result in strain localization in the concrete near the fiber ends, which may affect the crack distribution in the SFRC specimens.

References:

[1] Bentur A, Mindess S. Fiber reinforced cementitious composites. Cromwell Press,Trowbridge,Wiltshire, 2007.

[2] Banthia N, Nandakumar N. Crack growth resistance of hybrid fiber reinforced cement composites. Cement & Concrete Composites 25 (2003) 3–9.

[3] Banthia N, Sappakittipakorn M. Toughness enhancement in steel fiber reinforced concrete through fiber hybridization. Cement and Concrete Research 37 (2007) 1366–1372.

[4] Wang ZL, Wu LP, Wang LG. A study of constitutive relation and dynamic failure for SFRC in compression. Construction and Building Materials 24 (2010) 1358–1363.

[5] Thomas J, Ramaswamy A. Mechanical properties of steel fiber-reinforced concrete. ASCE Journal of Materials in Civil Engineering, 19 (2007) 385-392.

[6] Vandewalle L. Influence of tensile strength of steel fiber on toughness of high strength concrete, Proceedings of Third International Workshop on High-Performance Cement Composites (Mainz, Germany), H. W. Reinhardt and A. E. Naaman, eds., RILEM Publications, Bagneux, France, 1999, pp. 331-337.

[7] Johnston CD. Fiber-Reinforced Cements and Concretes, Gordon and Breach Science Publishers, Ottawa, Canada, 2001.

[8] Shah SP, Weiss J, Yang W. Shrinkage Cracking - Can It Be Prevented? , Concrete International, 20 (1998) 51-55.

[9] Harragan B, Gettu R, Martin M, Zerbino R. Uniaxial tension test for steel fiber reinforced concrete - a parametric study. Cement & Concrete Composites 25 (2003) 767–777.

[10] Wille K, El-Tawil S, Naaman A E. Preperties of strain hardening ultra-high performance fiber reinforced concrete (UHP-FRC) under direct tensile loading. Cement & Concrete Composites 48 (2006) 53-66.

[11] Mohammadi Y, Carkon-Azad R, Singh SP, Kaushik SK. Impact resistance of steel fibrous concrete containing fibers of mixed aspect ratio. Constr Build Mater 23(2009) 183–9.

[12] Wang ZL, Shi ZM, Wang JG. On the strength and toughness properties of SFRC under static-dynamic compression. Composites: Part B 42 (2011) 1285–1290.

[13] Wang ZL, Shi ZM, Wang JG. Experimental and numerical analysis on effect of fiber aspect ratio on mechanical properties of SRFC. Construction and Building Materials 24 (2010) 559–565.

[14] Teng TL, Chu YA, Chang FA, Shen BC, Cheng DS. Development and validation of numerical model of steel fiber reinforced concrete for high-velocity impact. Computational Materials Science 42 (2008) 90–99.

[15] Xu Z. Experimental and numerical study of dynamic material properties of fiber reinforced concrete. PhD thesis, the University of Western Australia. Dec 2011.

[16] Nieuwoudt PD. Time-dependent behaviour of cracked steel fiber reinforced concrete: from single fiber level to macroscopic level. PhD thesis, Stellenbosch University, 2016.

[17] Hallquist JO. LS-DYNA theoretical manual. Livermore, CA, USA: Livermore Software Technology Corporation; 2003.

[18] Thomas T. CEB-FIB Model Code 1990. Lausanne, Switzerland, design code edition, 1993.

[19] Cunha VMCF, Barros JAO, Sena Cruz JM. Pullout behavior of steel fibers in self-compacting concrete. Journal of Materials in Civil Engineering, 22 (2010) 1-9.

[20] Li V, Stang H. Interface property characterization and strengthening mechanisms in fiber reinforced cement based composites. Advanced Cement Based Materials, 6 (1997) 1-20.

[21] Kim DJ, El-Tawil S, Naaman AE. Rate-dependent tensile behavior of high performance fiber reinforced cementitious composites. Mater Struct 42 (2009) 399–414.

[22] Tran TK, Kim DJ. High strain rate effects on direct tensile behavior of high performance fiber reinforced cementitious composites. Cement & Concrete Composites 45 (2014) 186-200.